



ASME Accepted Manuscript Repository

Institutional Repository Cover Sheet

First

Last

ASME Paper Title:

Improving the Uncertainty of Exhaust Gas Temperature Measurements in Internal Combustion Engines

Authors:

Papaioannou, N., Leach, F., and Davy, M.

ASME Journal Title:

Journal of Engineering for Gas Turbines and Power

Volume/Issue: 142(7): 071007

Date of Publication (VOR* Online): 21/05/2020

ASME Digital Collection URL:

<https://asmedigitalcollection.asme.org/gasturbinespower/article-abstract/142/7/071007/1083898/Improving-the-Uncertainty-of-Exhaust-Gas?redirectedFrom=fulltext>

DOI: 10.1115/1.4047283

*VOR (version of record)

Abstract

Accurate measurement of exhaust gas temperature in internal combustion engines is a challenging task. The most common, and also the most practical, method of measurement is to insert a physical probe, for example a thermocouple or platinum resistance thermometer (PRT), directly into the exhaust flow. Historically, consideration of the measurement errors induced by this arrangement have focused on the effects of radiation and the loss of temporal resolution naturally associated with a probe of finite thermal inertia operating within a pulsating flow with a time varying heat input. However, a recent numerical and experimental study has shown that conduction errors may also have a significant effect on the measured exhaust gas temperature, with errors approaching ~ 80 K depending on engine operating conditions. In this work, the authors introduce a new temperature compensation method that can correct for the combined radiation, conduction and dynamic response errors introduced during the measurement and thereby reconstruct the “true” crank-angle resolved exhaust gas temperature to an estimated accuracy of ± 1.5 %. The significance of this result is demonstrated by consideration of a first law energy balance on an engine. It is shown that the exhaust gas enthalpy term is underestimated by 15–18 % when calculated using conventional time-averaged data as opposed to using the mass-average exhaust enthalpy that is obtained by combining the reconstructed temperature data with crank angle resolved exhaust flow rates predicted by a well-validated 1-D simulation.

Background

Exhaust gas temperature (EGT) is an important parameter in the design and monitoring processes of internal combustion engines. For example, inaccurate EGT measurements can result in efficiency penalties from underutilisation of the turbine and inefficiencies in managing exhaust gas after-treatment devices—catalyst conversion efficiency is dependent on their operating temperature and diesel particulate filters require exhaust gas temperature control for regeneration events. Energy balance analyses on internal combustion engines also highlight the need for accurate EGT measurement, especially when investigating the effects of different combustion strategies and piston materials [1-6], and numerical simulations require reliable experimental data for model validation [7].

Temperature measurements in internal combustion engines (ICEs) are usually carried out using intrusive methods, i.e. by immersing a sensor device, typically a thermocouple or platinum-resistance thermometer (PRT), directly into the flow of interest. However, these intrusive type sensors are subject to several sources of measurement errors namely: conduction, radiation and dynamic errors, each of which will be discussed in more detail in subsequent sections of this work. Alternative, non-intrusive methods include radiation thermometry and advanced laser based diagnostic techniques such as planar-laser induced fluorescence (PLIF) [8], laser induced grating spectroscopy (LIGS) [9] or a combination of both [10]. While these techniques do not suffer from the errors associated with intrusive methods, the associated cost, complexity and a general lack of robustness prevents them from widespread use outside of a research laboratory. This paper will thus concentrate on the use of thermocouple techniques.

Thermocouple measurements of exhaust gas temperature rely on the effective transfer of heat from the pulsating fluid flow to the sensor. This process has two caveats; first, the sensor indicates the temperature of the thermocouple junction and not the fluid's temperature which will be lower due to conduction and radiation heat transfer away from the junction. The effects of conduction and radiation errors in ICEs have been the subject of many studies in the past [11-16]. Figure 1 shows the various heat transfer modes that a thermocouple junction is exposed to when installed on the exhaust pipe of an ICE. This schematic assumes that the gas is at a higher temperature than the junction and the wall at a lower temperature. This is not always the case and simulations have shown that during the period that the exhaust valves are closed, the junction can be at a higher temperature than the surrounding gas [15].

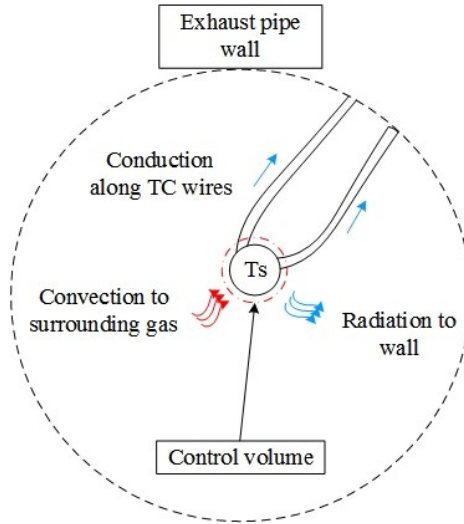


Figure 1: Heat transfer on a thermocouple junction installed in a pipe with internal flow. Adapted from [15].

The second caveat is that, the heat transfer rate from the surrounding gas to the sensor is finite, which means that the sensor will indicate changes in temperature with some delay. This is the cause of the dynamic error under unsteady temperature measurements which scales with the size of the sensor. The dynamic error is thus the inability of the sensor to follow the changes of the measured parameter, in this case, temperature. A measure of the dynamic error of the sensor is the time-constant (τ) and is defined below:

$$\tau = \frac{mc_p}{hA_s} \quad (1)$$

m and c_p are the mass and the heat capacity and h and A_s the heat transfer coefficient and the surface area of the thermocouple junction. This equation shows that the time-constant is both a function of the sensor size as well as the flow's properties which makes its estimation challenging, and an area of extensive research [17-21].

Previously, comparative experiments were conducted on a single-cylinder diesel engine (refer to Table 2 for details) where the exhaust gas temperature was logged using both a fast-response thermocouple probe (comprising of a 50.8 μm , a 127 μm and a 254 μm fine-wire thermocouple) and a standard 3 mm sheathed thermocouple (refer to Table 1) [15]. It should be noted that only K-type thermocouples were used for this work. For more details regarding the uncertainty of these sensors please refer to the *Calibration* section.

The results, presented in Figure 2, showed that for both of the speed/load conditions tested the time-average EGT calculated from the fast-response probe is lower than the value reported by a 3 mm reference thermocouple, a result that was initially counter-intuitive. Further numerical, studies supported these findings and demonstrated that the observed experimental discrepancies (up to ~ 80 K) were attributable to the combined effects of conduction error and the smaller thermal mass of the fine-wire thermocouples.

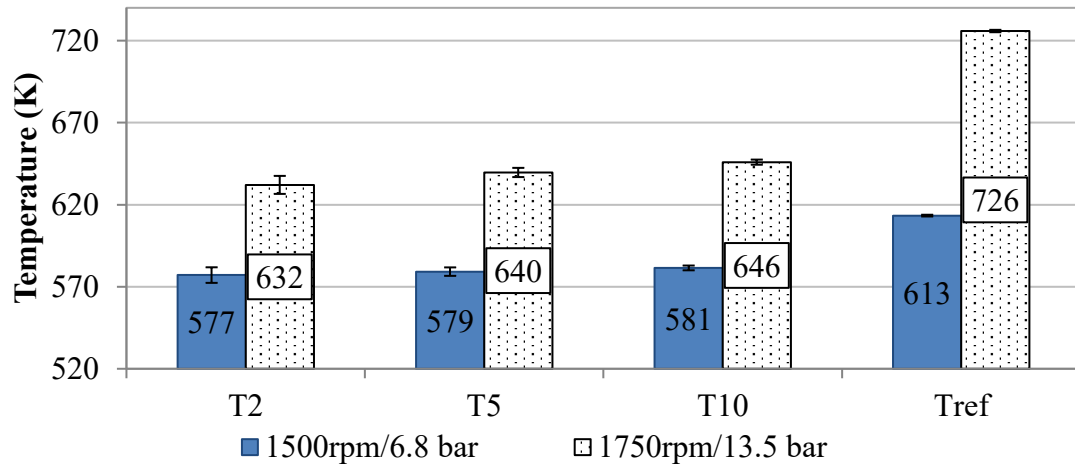


Figure 2: Experimental time-average exhaust temperatures for the different thermocouple sizes for both speed/load conditions. T2 is the temperature of the 50.8 μm , T5 the temperature of the 127 μm and T10 the temperature of the 254 μm thermocouple. Tref shows the temperature of the 3 mm sheathed thermocouple. The error bars indicate the 95 % confidence limits.

More specifically, it was found that during the period that the valves are closed, heat transfer via conduction and radiation dominates the energy transfer process to the thermocouple junction. This is true regardless of junction size. However, the fine-wire thermocouples cool faster compared to the surrounding gas due to their small thermal mass whereas the opposite is true for the reference thermocouple (the magnitude of the conduction losses are similar for fine-wire and the reference thermocouples). It was also shown that despite the small size of the fine-wire thermocouples, there is still a non-negligible dynamic error associated with the sensors, and thus that some form of correction is required to estimate the “true” exhaust gas temperature.

A temperature reconstruction technique was developed, based on the work of Tagawa et al., [18] which corrected for the dynamic error using simulated exhaust temperature signals, however, in this earlier work the conduction and radiation errors were ignored. The results of the reconstruction technique can be seen in Figure 3, where the solid line represents the “true” gas temperature, the dotted line the reconstructed temperature and the blue and red lines the simulated thermocouple signals that were used for the reconstruction. Considering the overall good agreement and that the deviation in peak EGT in the order of 1.8 %, this technique shows very promising results.

Further to this, knowledge of the “true” gas temperature, which can be provided with the use of the aforementioned reconstruction technique also allows for a more accurate estimation of exhaust gas enthalpy. Therefore, in this paper, we first present a method for reducing the inherent dynamic, conduction and radiation errors associated with the measurement process thus resulting in a more accurate indication of the “true” gas temperature and secondly, we show how this then affects the estimation of exhaust enthalpy on an internal combustion engine.

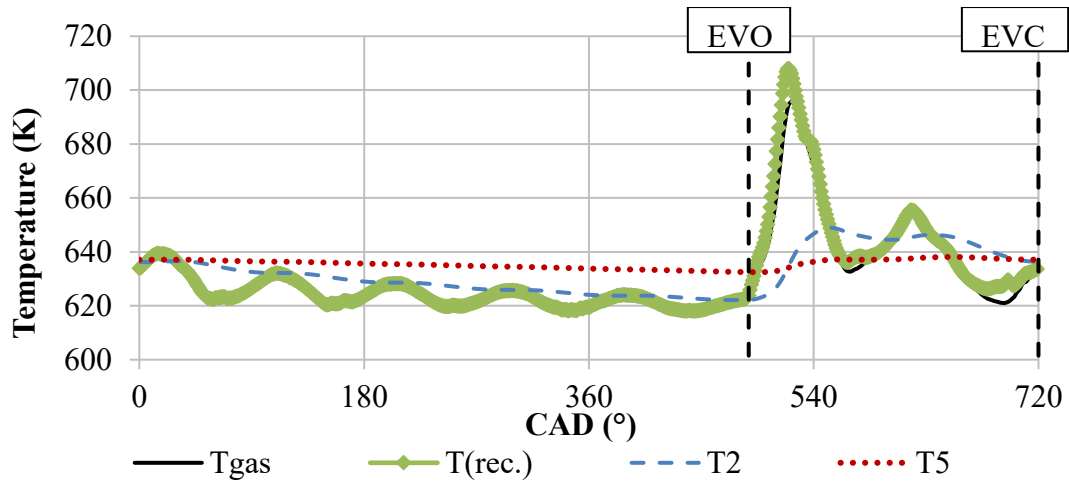


Figure 3: Reconstructed gas temperature results using simulated thermocouple signals. The solid line indicates the “true” gas temperature and the T2 and T5 lines show the simulated thermocouple signals used for in the reconstruction.

Numerical methodology

Lumped capacitance thermocouple model

The development and validation of the reconstruction method was completed using simulated thermocouple signals. These signals were created using a 1-D lumped capacitance thermocouple model and the gas temperature inputs to the thermocouple model, derived from simulations carried out on a commercially available one-dimensional code [23], represent the so-called “true” gas temperature against which the accuracy of the reconstruction will be tested. Details of the 1-D model validation can be found in [15].

The thermocouple model assumes that a uniform temperature distribution exists over the cross-sectional area of the exhaust pipe and that there is no variation in temperature along the radial and circumferential direction of the thermocouple. The exhaust wall temperature was also assumed to remain constant, based on experimental measurements [15]. Table 1 details the geometrical assumptions made for each thermocouple junction along with the Nusselt number correlations used following the work of Whitaker [22]. Further details on the modelling approach can be found in [15].

Table 1: Characteristics of modelled K-type thermocouples

Thermocouple diameter	Nusselt correlation	Junction geometry	Biot number
0.0508 mm (T2)	Sphere	Bead	0.000165
0.127 mm (T5)	Tube	Butt-welded	0.000325
0.254 mm (T10)	Tube	Butt-welded	0.000396
3 mm (Tref)	Tube	Sheath	0.000528

Temperature reconstruction method

In previous work by this study’s authors [15], the reconstruction method only corrected for the dynamic errors and ignored the effects of radiation and conduction following the work of Tagawa *et al.* [18]. This technique estimates the thermocouple time-constants by solving a simultaneous system of equations based on an energy balance approach while minimising the time-average difference between the two thermocouple temperatures. The simultaneous system of equations to be solved, can be seen below:

$$\left. \begin{aligned} T_{g1} &= T_{s1} + \tau_1 \frac{dT_{s1}}{dt}, \\ T_{g2} &= T_{s2} + \tau_2 \frac{dT_{s2}}{dt}, \end{aligned} \right\} \quad (2)$$

where T_s is the temperature indicated by the thermocouple and τ the thermocouple's time-constant.

Expanding on this logic, Equation 2 was adapted to include the radiation and conduction error terms, based on an energy balance approach around the thermocouple junction (Figure 1). Equation 2, then becomes:

$$\left. \begin{aligned} T_{g1} &= T_{s1} + \tau_1 C_1, \\ T_{g2} &= T_{s2} + \tau_2 C_2, \end{aligned} \right\} \quad (3)$$

Where the parameter C is including all the sources of measurement error and is equal to:

$$\begin{array}{ccc} \text{Radiation} & \text{Conduction} & \text{Dynamic} \\ \underbrace{\hspace{1cm}} & \underbrace{\hspace{1cm}} & \underbrace{\hspace{1cm}} \\ C = \beta(T_s^4 - T_w^4) + \gamma(T_s - T_w) + \frac{dT_s}{dt} \end{array} \quad (4)$$

Where T_w is the exhaust pipe wall temperature and the parameters β and γ are equal to:

$$\beta = \frac{\sigma \varepsilon A_s}{mc_p} \quad (5)$$

$$\gamma = \frac{2A_{csa}k}{mc_p L} \quad (6)$$

where σ is the Stefan-Boltzmann constant, ε the emissivity of the thermocouple material and k , m and c_p are the thermal conductivity, mass and heat capacity of the thermocouple material respectively. A_s is the junction surface area and A_{csa} denotes the cross-sectional area of the thermocouple wire. Finally L denotes the length over which the conduction error is calculated.

Minimizing the time-averaged temperature difference between the two local gas temperatures (i.e. T_{g1} and T_{g2}) results in the time-constants τ_1 and τ_2 presented Equation 7 below:

$$\left. \begin{aligned} \tau_1 &= \frac{(\sum C_2^2)(\sum C_1 \Delta T) - (\sum C_2 \Delta T)(\sum C_1 C_2)}{(\sum C_2^2)(\sum C_1^2) - (\sum C_1 C_2)^2}, \\ \tau_2 &= \frac{(\sum C_1 C_2)(\sum C_1 \Delta T) - (\sum C_2 \Delta T)(\sum C_1^2)}{(\sum C_2^2)(\sum C_1^2) - (\sum C_1 C_2)^2}, \end{aligned} \right\} \quad (7)$$

where Σ indicates the moving average filter process and ΔT is the temperature difference between the two thermocouple signals used for the reconstruction.

The results of Equation 7 are highly sensitive to the averaging process since thermocouple signals are subject to measurement noise and the derivative term in Equation 4 will tend to decrease the signal-to-noise ratio thus resulting in over-compensation of the temperature signal. Consequently, some form of noise reduction is necessary. Tagawa *et al.* [18] employed a central sliding moving average window to remove signal noise, with the size of the window providing a compromise between temporal resolution and non-physical values from the resulting time-constants (i.e. negative values for τ). More specifically, as the window

size is increased, the effect of averaging is more pronounced and the resulting time-constants approach their time-average ($\bar{\tau}$), rather their instantaneous values (τ).

In this work the averaging process varied during the cycle, in order to minimise the effects of averaging on the instantaneous values of τ . As the gas in the exhaust is essentially stationary for the period that the valves are closed (EVC) (Figure 4), a single averaging window was used during the EVC period. Considering the inherent dynamic error of temperature sensors, the indicated value at a given time will be a result of the flow conditions that the sensor has been exposed to in the past. In the period that the exhaust valve is open, and particularly close to the blowdown period, the time-constant will be rapidly changing. Therefore, during the EVO period an exponential moving average window—which is more suited to predict rapidly changing values than a simple moving average—was used in the estimation of the time-constant. Equation 8 refers [24].

$$f(t) = \zeta g(t) + (1 - \zeta)f(t - 1) \quad (8)$$

where $f(t)$ is the filtered output, $g(t)$ is the input value and ζ is the weight factor.

The weight factor determines the importance of the past values on the filtered output, with a value of 1 implying that the same weight is given to all past data (i.e. simple moving average). In this work, ζ was set to $\zeta = 0.08$, as this value was found to provide the best compromise between temporal resolution and non-negative time-constant values for the T2/T5 thermocouple combination. This pair was used as it has the highest temporal resolution of the thermocouples tested and as such the potential to provide the most accurate reconstruction results. This is discussed further in the next section.

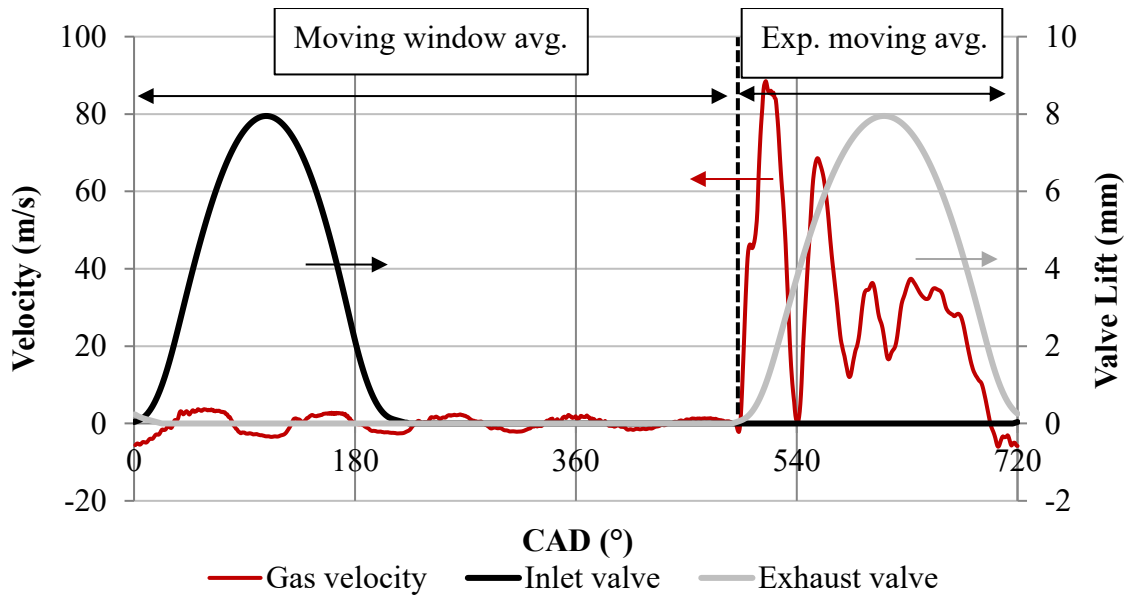


Figure 4: Simulated gas velocity profile for the conditions tested. The different averaging methods used are also shown for the two valve events.

The results of the reconstruction method were validated in two ways. First, considering the construction of the fast-response probe (Table 1) the reconstruction method can be validated qualitatively against the different thermocouple pairs (refer to next section). Secondly, since the 1-D model provides an indication of the “true” exhaust gas temperature, this was used to create simulated thermocouple signals using the aforementioned lumped capacitance model. These simulated thermocouple signals were then used to reconstruct the original signal provided by the 1-D model. The schematic below shows the methodology used for the temperature reconstruction validation.

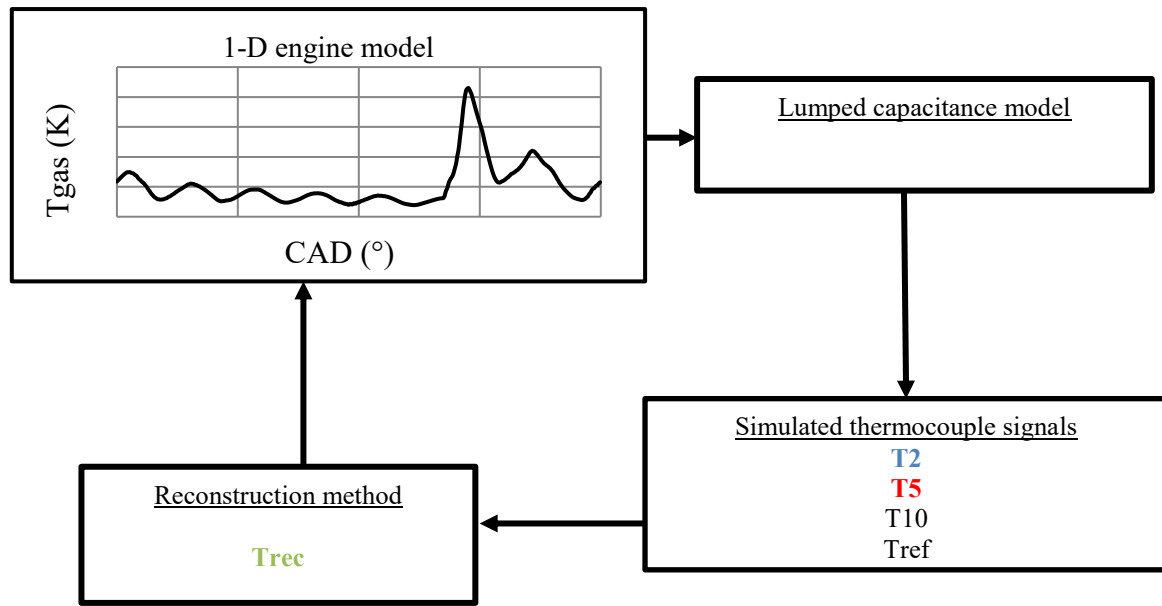


Figure 5: Validation methodology of reconstruction method.

Experimental methodology

Engine test conditions

The experimental work carried out to support the results presented in this paper was completed on a single-cylinder diesel engine and is presented in detail in previous publication [15]. The engine configuration along with the fuel specification used is presented in Table 2. The engine was operated at two speed/load conditions as can be seen in Table 3. A 3 mm sheathed K-type thermocouple was used to measure the exhaust temperature shown in Table 3.

Table 2 Engine configuration and fuel specifications

Parameter	Specification
Bore × Stroke (mm)	83 × 92.4
Displacement (cm ³)	500
Valves per cylinder (-)	2 intake, 2 exhaust
Fuel system (-)	Common rail
Fuel cetane number (-)	52
Fuel Sulphur content (mg/kg)	6.5
Fuel LHV (kJ/g)	42.7

Table 3: Engine test conditions

Test point	1500 rpm/6.8 bar nIMEP	1750 rpm/13.5 bar nIMEP
Engine speed (rpm)	1500	1750
nIMEP (bar)	6.8	13.5
Measured exhaust temperature (K)	623	753
Wall Temperature (K)	506	589

Calibration

All thermocouples were initially checked for linearity using a water bath calibration in the range of 298-362 K, with good agreement. In order to test the thermocouples in the temperature range expected to observe on the engine, miniature oven capable of simultaneously supporting the fast-response probe and the reference thermocouple was designed and built for this higher temperature calibration. Three tests were carried out in the range of 473-773 K with the data acquisition procedure starting once the reference thermocouple reached the target temperature and all reading were constant.

The results of this calibration are presented in Figure 6. The y-axis indicates the readings for the fine-wire thermocouples and the x-axis the reference thermocouple readings. The error bars represent the 95 % confidence limits and the black line the unity slope line of the reference thermocouple. The observed discrepancies at the highest temperatures are attributed to the much faster cooling rate of the oven compared to the rate of heating input at these temperatures. Consequently, due to the higher thermal mass of the reference thermocouple this resulted in a lower apparent temperature compared to the fine-wire thermocouples.

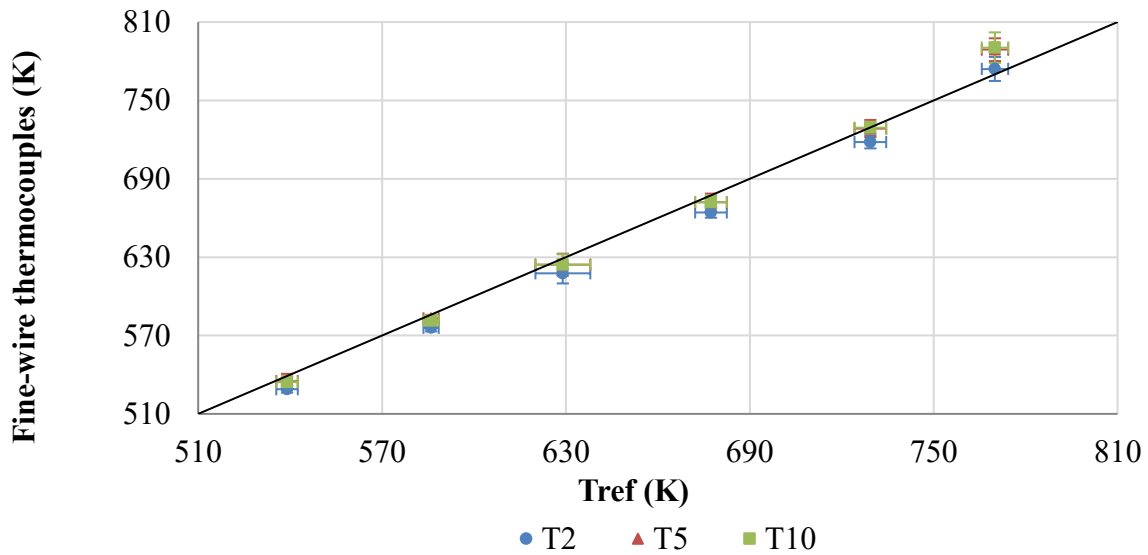


Figure 6: Calibration results. Error bars indicate the 95% confidence limits over three tests.

Results and discussion

Effect of time-constant of temperature reconstruction

As already mentioned, the dynamic error is dependent on the sensor's time-constant (τ) which in turn is dependent on the physical characteristics of the sensor and the local flow conditions driving the heat transfer process (Equation 1). A sensor with a small thermal mass (i.e. mc_p) will have a smaller time-constant and be able to respond to temperature fluctuations faster than a sensor with a high thermal mass. Equally for a given thermal mass, an increase in the convective heat transfer coefficient h will reduce the time-constant of the sensor as the heat transfer process is accelerated. Thus, it is reasonable to expect that the maximum value of the sensor time-constant during the cycle will occur during the EVC period where the gas velocities are negligible (Figure 4), and that substantially lower time-constants will be seen during the blowdown and EVO periods.

Figure 7 shows the reconstructed time-constants for the 1500 rpm/6.8 bar nIMEP conditions, for the three bare-wire thermocouples used, T2, T5, and T10 (refer to Table 1). The time-constant for each thermocouple was calculated twice using all possible combinations for the three thermocouples. For example, τ_2 (2/5) in Figure 7 is the time-constant of thermocouple T2 as calculated by Equation 7 using thermocouples T2 and T5. Thermocouples T2 and T10 can also provide an indication of τ_2 and this is also shown in Figure 7 by τ_2 (2/10). This then provides a qualitative way of validating the accuracy of the reconstruction method. The solid line indicates the "true" time-constants as calculated in the lumped capacitance model. The error bands on the "true" time-constant are associated with the uncertainties in the Nusselt number correlation which in this case are ~25 % [22]. The observed undulations on the "true" time-constants are linked to the pressure pulses found in the exhaust of the engine and captured

by the exhaust pressure transducer; a measurement that is used as a boundary condition in the 1-D numerical model used to provide the “true” gas temperature profile.

The time-constant is known to increase with the size of the thermocouple a trend that is captured by the reconstruction method, with the T2 thermocouple having the smallest time-constant and the T10 thermocouple having the highest. Overall the calculated time-constants agree well with the “true” values irrespective of junction size and pair combination, especially during the period where the exhaust valves are closed (i.e. 0-488 CAD). During the EVO period, however, the accuracy of the reconstructed time-constants is driven by the junction pair combination. More specifically, time-constants calculated using the T5 and T10 thermocouples (i.e. Figure 7b and 7c) result in notable deviations from the “true” values, both in terms of time shift and magnitude. This is attributed to the slower response of both thermocouples and their reduced temporal resolution.

Apart from the obvious effects of this phase delay on the reconstructed temperature, the smaller time-constants predicted with the 5/10 pair will under-predict the dynamic error of the sensor and will thus result in an under-prediction of the “true” gas temperature. Both of these points will result in a lower estimation of the exhaust enthalpy. On the other hand, reconstruction results using the T2 thermocouple, do not show similar discrepancies, irrespective of the size of the second junction. This can be due to the fact that the T2 thermocouple has a high enough dynamic response to compensate for the negative effects introduced by the T5 and T10 thermocouples in terms of temporal resolution.

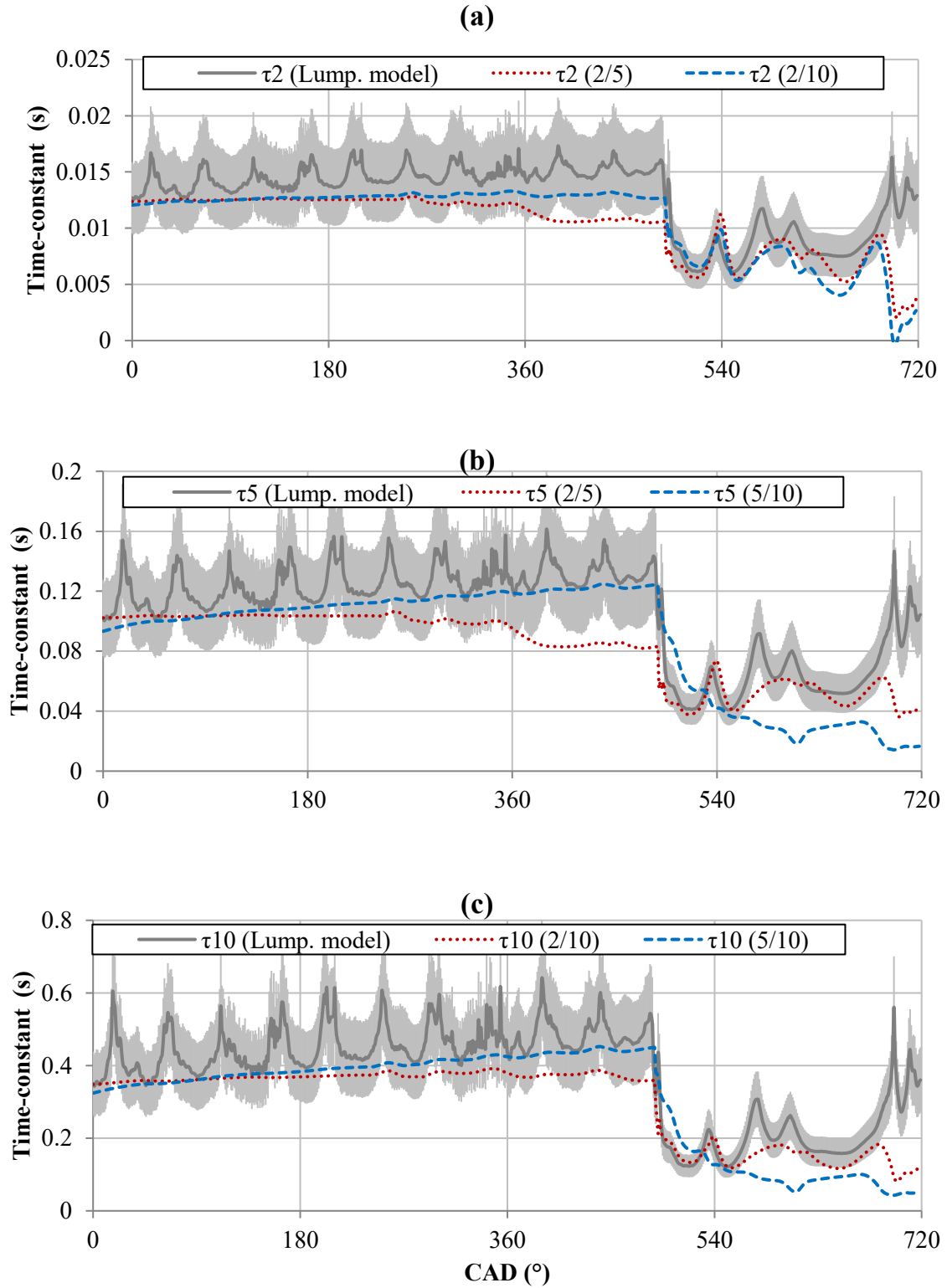


Figure 7: Typical time-constant estimation for different size thermocouples using different pair combinations. The solid line indicates the “true” time-constant and the light grey band the error associated with the Nusselt number correlation used.

The effect of different thermocouple pair combinations on the temperature reconstruction can be seen in Figure 8, where the solid line indicates the “true” gas temperature as provided from the 1-D simulations. The results show that when the T2 thermocouple is

part of the thermocouple pair, the temperature reconstruction is in closer agreement to the “true” gas temperature, a result that is also reflected by the reconstructed time-constants presented in Figure 7. Equally, the discrepancies observed in Figure 7a 7b and 7c in terms of time-constant prediction, when the T5 and T10 thermocouples were used, can also be seen in the reconstructed signals (T_{rec} (5/10) in Figure 8). For example, the over-prediction in the time-constant values seen around 500 CAD in Figure 7b and 7c is translated, according to Equation 3 to an over-prediction in peak temperature and similarly, the under-prediction in time-constants around 610 CAD, resulting in a temperature under prediction of ~ 25 K.

Figure 8 thus shows that when the 5/10 pair is used the accuracy of the reconstruction is reduced, despite the potential benefits that these thermocouples would offer in terms of service-life due to their bigger size. It is also noted that similar trends were observed at the higher load/speed conditions. Consequently, the reconstruction results presented from this point onwards will be those obtained using the 2/5 pair. The following section will present the results of the reconstruction method according to Equation 3.

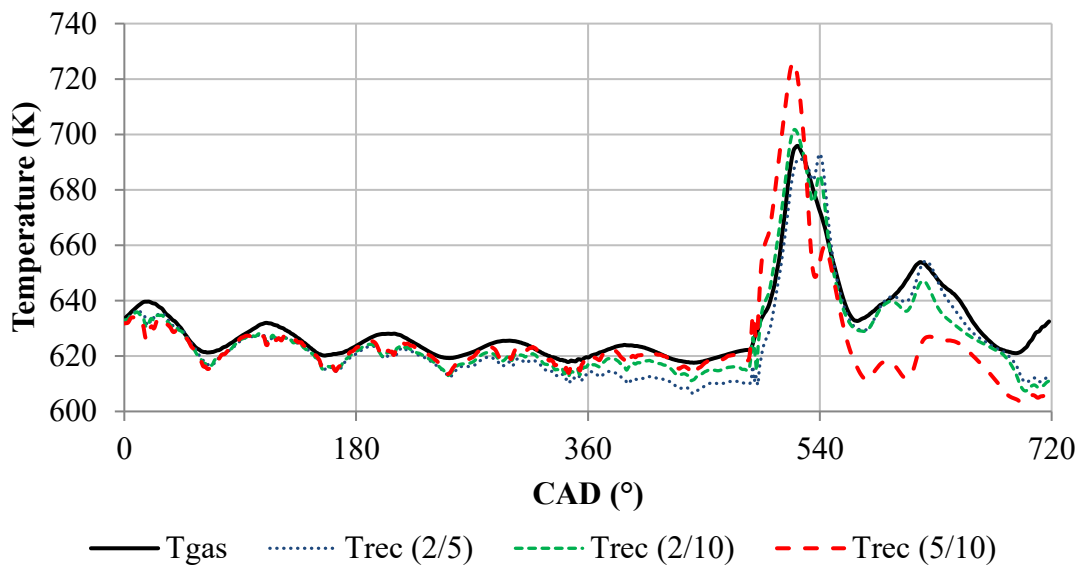


Figure 8: Typical temperature reconstruction results using different thermocouple pair combinations. The black line indicates the “true” gas temperature

Temperature reconstruction

The combined effects of convection, conduction and radiation will affect the thermocouple response during the cycle, as the cooling/heating rates of the junction will change due to the additional energy transfer terms considered—in terms of modelling when conduction and radiation are not considered the junction is losing or gaining energy due to convection to the cooler gas during the EVC period. The reconstruction method thus needs to be capable of capturing this change in response linked to conduction and radiation errors, on top of the effects introduced by the thermocouple’s thermal mass—it is recalled that this is accounted for mathematically using the term C in Equation 4. It should be noted that for the work presented here the “true” time-constants are not expected to change by incorporating the effects of conduction and radiation as the properties of the thermocouples have been taken to be independent of temperature and thus a change in junction surface temperature will have no effect. Consequently, any change in the “true” time-constant will be due to changes in exhaust gas velocity alone.

The reconstructed time-constants, including conduction and radiation errors, for the T2 thermocouple, under the 1500 rpm/6.8 bar nIMEP and the 1750 rpm/13.5 bar nIMEP conditions, can be seen in Figure 9 and Figure 10 respectively (circular markers). The reconstructed time-constants ignoring conduction and radiation error are also plotted for comparison (dotted line). For the lower speed/load case the reconstructed time-constants agree well with their “true” values throughout the cycle independent of the effects of conduction and radiation. It can also be seen that for the EVC duration, the effect of conduction and radiation is to reduce the value of the reconstructed time-constant. This is expected as conduction and radiation will increase the rate of change in temperature (in this case a reduction) which according to Equation 8, results in a smaller time-constant. During the EVO event, a similarly good agreement is observed in the reconstructed time-constants, irrespective of conduction and radiation effects, except from a discrepancy observed at ~ 710 CAD, when conduction and radiation is considered. This is thought to be a result of the rapid change in flow conditions observed at this point (Figure 4); this is considered to be linked to the aforementioned

limitations of the averaging process. A lower value of ζ is expected to improve this discrepancy but with a loss of accuracy at the earlier stages of the EVO event, which is not desirable, since at this point peak mass flow rates are occurring and consequently this will have the biggest effect on mass-average exhaust enthalpy. Similar results were also observed for the T5 thermocouple and are thus not presented here.

Under the higher speed/load conditions, the time-constant is reduced, in agreement with the increased heat transfer coefficient, associated with the higher exhaust gas velocities. The agreement with the “true” values is equally good to the lower speed/load case, with the effects of averaging being responsible for the deviations observed during the EVO period. Again, the effect of conduction and radiation, results in a lower time-constant value during the EVC period compared to the case where conduction and radiation are ignored which has already been seen for the lower speed/load conditions. When the valves open, the time-constants including the effects of conduction and radiation, present generally good agreement during this event. A similar under-prediction to the 1500 rpm/6.8 bar nIMEP case is also observed around 710 CAD. The effects of averaging are more prevalent under these conditions as the velocity of the gases and the changes in temperature are increased. This is more profound for the case where conduction and radiation effects are not taken into account, where the reconstructed time-constant is taking negative values at the time of EVO. This is obviously not feasible and the temperature reconstruction results at this point should not be trusted. Again, this indicates the compromise necessary on the averaging process; less averaging increases the temporal resolution but can result in negative time-constant and vice-versa.

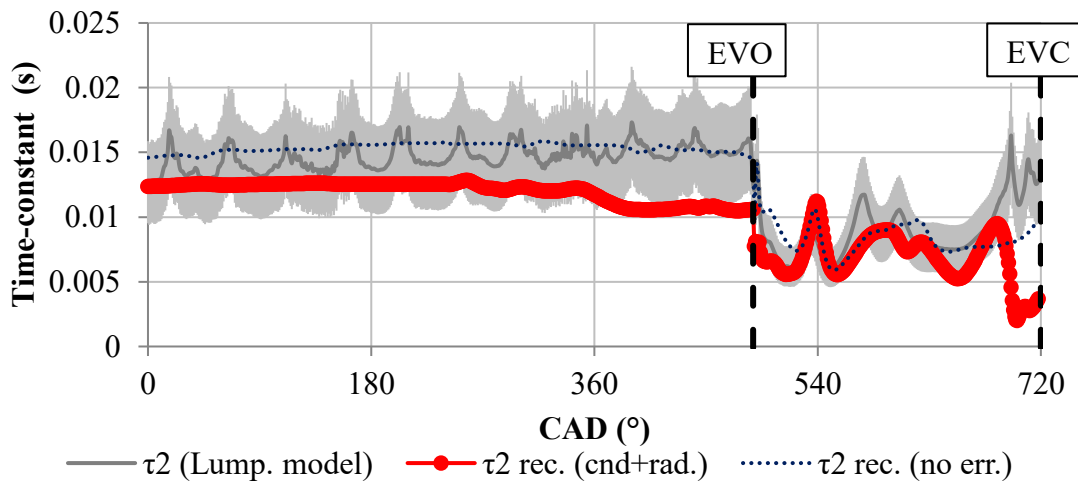


Figure 9: Time-constant reconstructed values for the T2 thermocouple under the 1500 rpm/6.8 bar nIMEP case (Equation 7). The dotted line indicates the reconstructed time-constant ignoring conduction and radiation errors. The solid line indicates the “true” time-constant and the error bands the uncertainty associated with the Nusselt number correlation used.

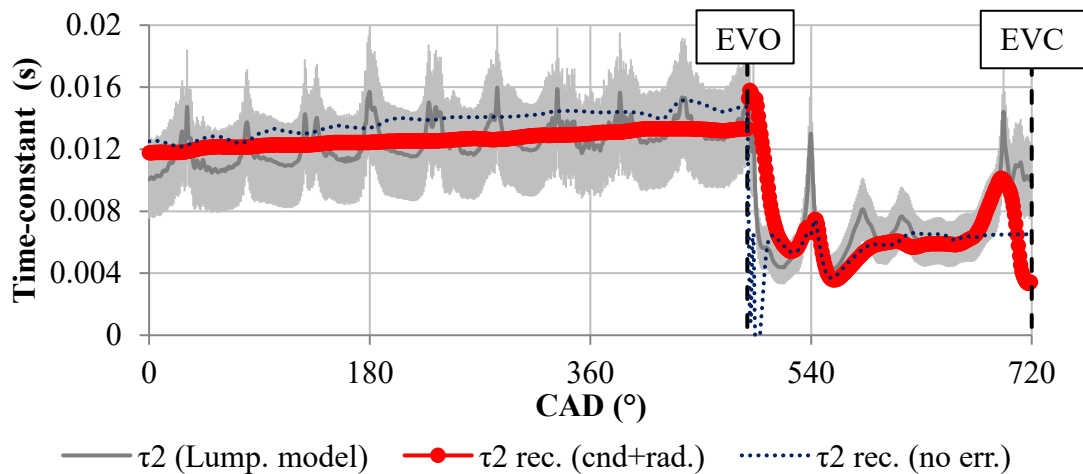


Figure 10: Time-constant reconstructed values for the T2 thermocouple under the 1750 rpm/13.5 bar nIMEP case (Equation 7). The dotted line indicates the reconstructed time-constant ignoring conduction and radiation errors. The solid line indicates the “true” time-constant and the error bands the uncertainty associated with the Nusselt number correlation used.

The temperature reconstruction results, including conduction and radiation effects, for the two speed/load conditions can be seen in Figure 11 and Figure 12. Following the good agreement observed with the time constants, the reconstructed temperature shows equally good agreement to the “true” values, independent of load/speed condition. Comparing the two graphs it is immediately clear that the effects of conduction are more pronounced under the 1500 rpm/6.8 bar nIMEP case. Despite the higher temperature gradient between the gas and the wall at higher speed/load conditions, 390 K compared to 357 K under the lower speed/load observed experimentally, the peak temperature and the EVO frequency are increased which results in a reduction in energy losses during the EVC period and therefore to a higher indicated temperature. This would perhaps indicate that at even higher load/speed conditions the effect of conduction reduces further.

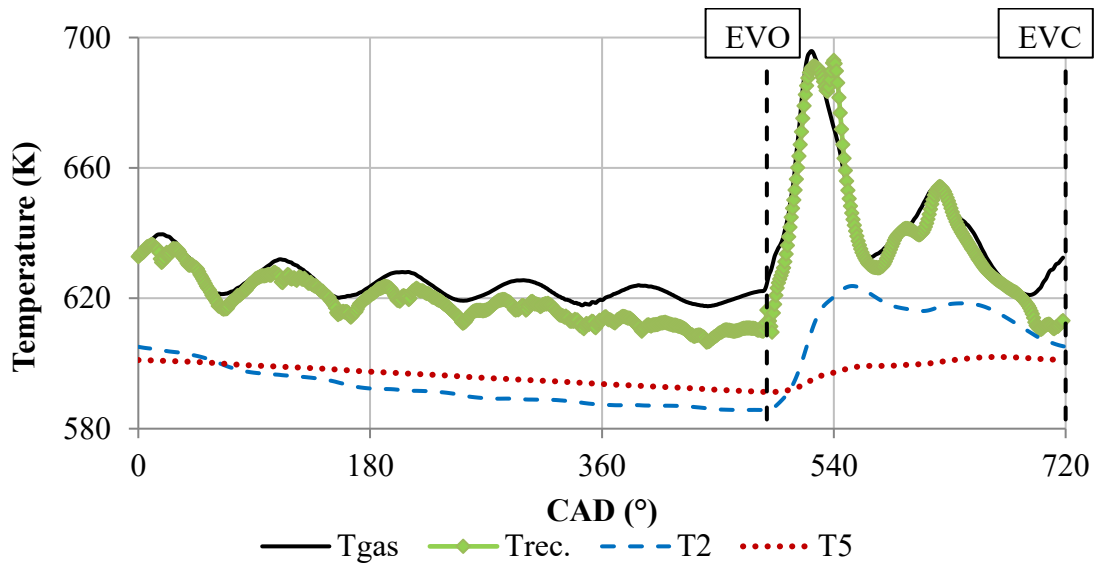


Figure 11: Temperature reconstruction results including conduction and radiation error for the 1500 rpm/6.8 bar nIMEP case (Equation 3). The dashed and dotted lines show the thermocouple signals used for the reconstruction.

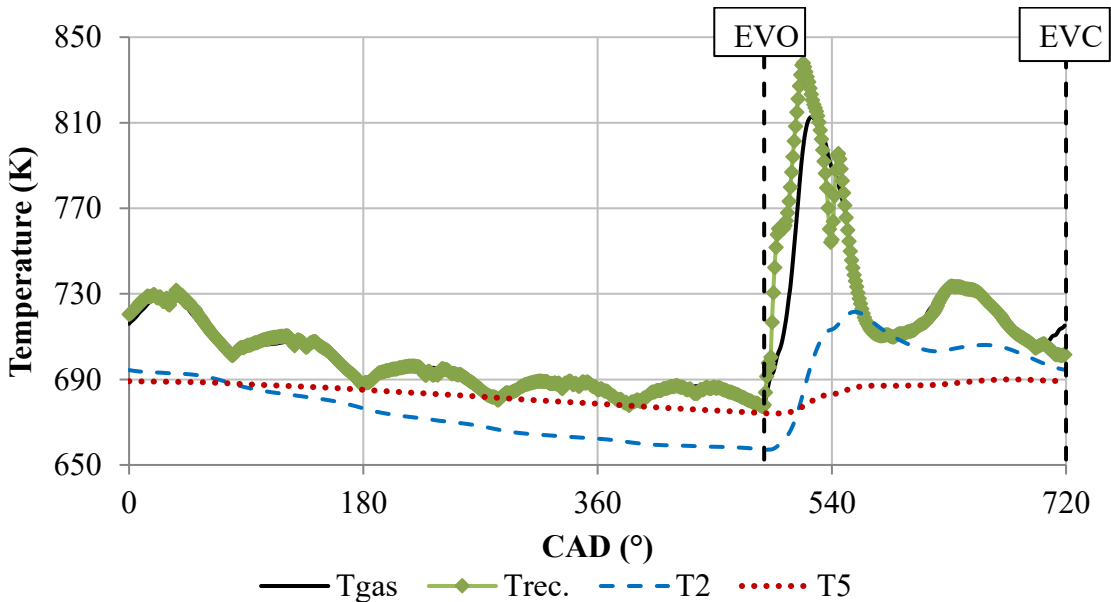


Figure 12: Temperature reconstruction results including conduction and radiation error for the 1750 rpm/13.5 bar nIMEP case (Equation 3). The dashed and dotted lines show the thermocouple signals used for the reconstruction.

As already observed, any discrepancies in the reconstructed temperatures are due to deviations in the reconstructed time-constants. More specifically, the under-prediction in the reconstructed time-constants, presented in Figure 9 and Figure 10 around 710 CAD is translated in a lower reconstructed temperature at this point. However, in terms of exhaust enthalpy estimation, this is not expected to affect the results significantly as the mass-flow rates at this point are approaching zero (Figure 13). The higher discrepancy during the EVO period is observed for the higher speed/load case and is attributed to the over-prediction of the time-constant at ~525 CAD (Figure 10) which indicates a higher dynamic error that the reconstruction method is consequently overcompensating. However, these discrepancies are translated to a maximum temperature deviation of 0.2 %, for the 1500 rpm/6.8 bar nIMEP case, and 3 %, for the 1750 rpm/13.5 bar nIMEP case.

These results are significant considering that the maximum temperature error is reduced by 12 and 14 percentage points under the higher and lower load conditions respectively. Being able to recover the “true” gas temperature from thermocouple signals allows, with knowledge of the instantaneous mass flow rate, for the estimation of the mass-average exhaust enthalpy as shown in Equation 6. The following section will present and compare first the mass and time-average enthalpies and then their effect on an energy balance calculation for the test conditions presented.

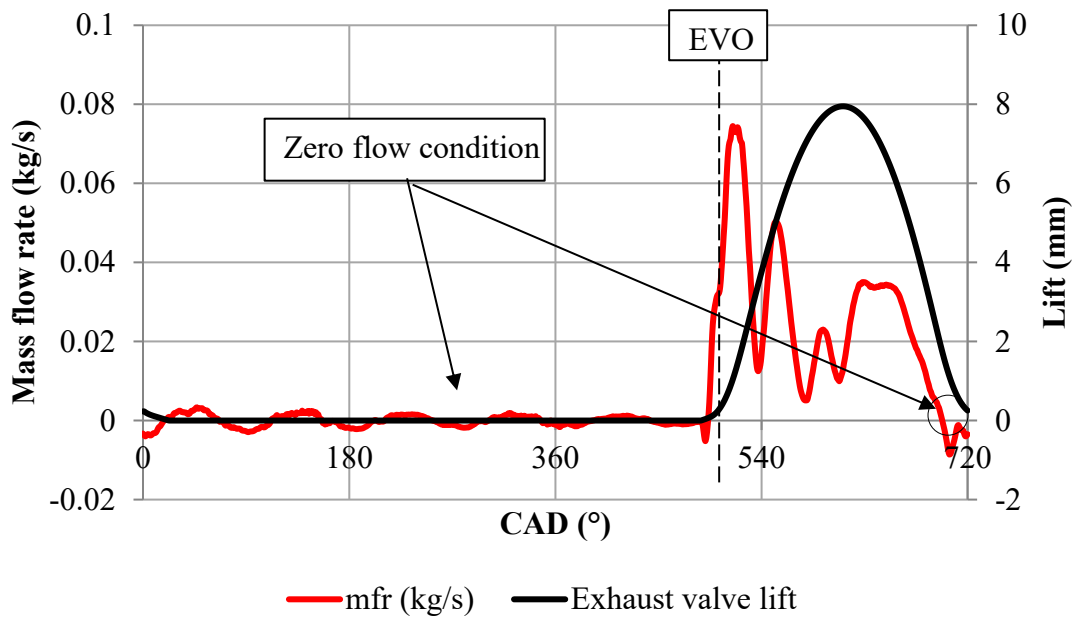


Figure 13: Modelled exhaust mass flow rate. Errors in temperature reconstruction at points of zero flow will not affect the accuracy of the mass-average enthalpy calculation.

Mass-average exhaust enthalpy flow calculation

The previous section has shown how the exhaust temperature measurement can be under predicted when the signal from temperature sensors is not corrected for the inherent dynamic, conduction and radiation errors associated with the measurement process. The significance of this result is now illustrated by consideration of the exhaust gas enthalpy term within a first law energy balance applied to a single cylinder research engine. Estimation of exhaust enthalpy requires knowledge of temperature and mass flow rate in the exhaust manifold.

Commonly, time-average values for both of these parameters are used as indicated in Equation 9, where c_p is the heat capacity of the exhaust gases (this is usually assumed to be independent of temperature), \bar{m}_{exh} is the time-average mass flow rate of the exhaust stream, \bar{T}_{exh} is the time-average exhaust temperature and T_0 is the inlet gas temperature.

$$\bar{Q}_{exh} = \bar{m}_{exh} c_p (\bar{T}_{exh} - T_0) \quad (9)$$

The time-average exhaust temperature (\bar{T}_{exh}) and mass flow rate (\bar{m}_{exh}) are calculated according to the following equations.

$$\bar{T}_{exh} = \int_0^{720} T_{exh} d\theta / \int_0^{720} d\theta \quad (10)$$

$$\bar{m}_{exh} = \int_0^{720} \dot{m}_{exh} d\theta / \int_0^{720} d\theta \quad (11)$$

where the limits of the integrals represent the cycle duration in crank-angle degrees.

However, the expulsion of exhaust gases during the cycle is a highly dynamic event and Caton *et al.* [5] have shown that time-average exhaust temperature can lead to significant under-prediction of the “true” exhaust enthalpy. Caton and co-workers suggest that a better method for estimating the exhaust enthalpy would be to use the instantaneous values for temperature and mass flow rate (i.e. $\dot{m}_{exh}(\theta)$). The *mass-averaged* exhaust enthalpy would then be calculated as follows:

$$\hat{Q}_{exh} = \dot{m}_{exh}(\theta) c_p (\hat{T}_{exh} - T_0) \quad (12)$$

where θ indicates the crank angle, and (\hat{T}_{exh}) the mass-average exhaust temperature. The latter is calculated according to Equation 13. It should be noted that the integration in this case is only carried out for the period that the exhaust valves are open.

$$\hat{T}_{exh} = \int_{EVO}^{EVC} \dot{m}_{exh}(\theta) T_{exh} d\theta / \int_{EVO}^{EVC} \dot{m}_{exh}(\theta) d\theta \quad (13)$$

Figure 14 shows a comparison of average exhaust temperatures, calculated on a different basis for the two speed/load conditions presented above. The red and green markers represent the time-average (Equation 10) and mass-average (Equation 13) temperatures and the blue colour represents a typical time-average temperature reading using a standard 3 mm sheathed thermocouple.

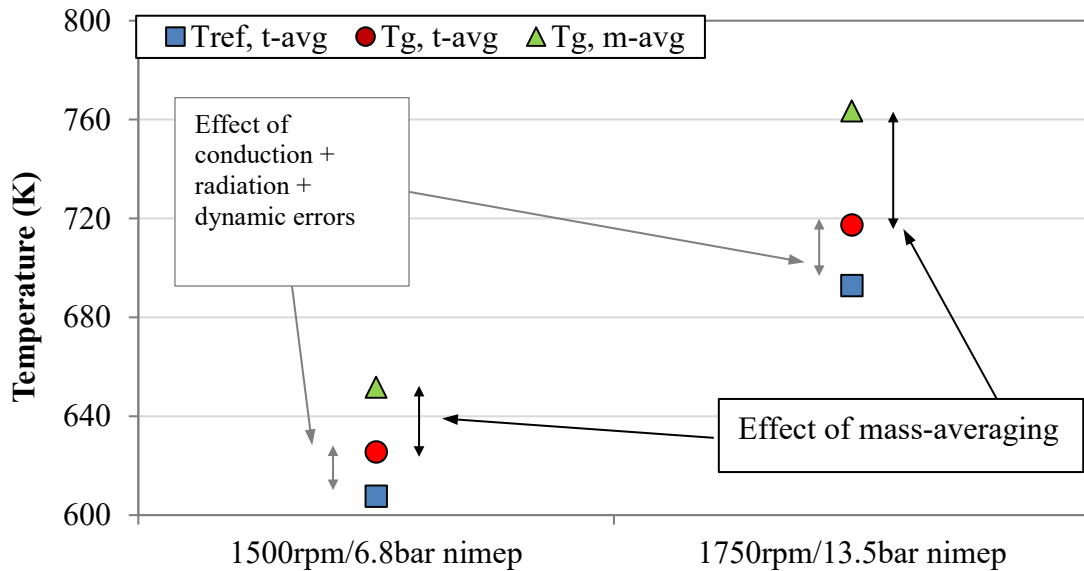


Figure 14: Average exhaust temperatures calculated on a different basis. The red colour indicates the time-average temperature (Equation 3) and the green colour the mass-average temperature (Equation 6). The blue colour indicates a typical temperature reading using a 3mm sheathed thermocouple.

As expected, the thermocouple reading is the lowest due to the conduction, radiation and dynamic errors discussed previously. What is interesting to note however, is the significant difference between the time and mass-average temperatures which is as high

as 40 K at the higher load conditions (~5 %). Considering a typical exhaust temperature profile (e.g. Figure 8), a time-averaging process over the whole cycle will tend to be skewed by the lower temperatures of the thermocouple junction due to the dominating conduction and radiation heat transfer observed during the EVC duration [15], which will result in an under-prediction of the time-average temperature. Note that this will be true even if the “true” gas temperature is known (e.g. red markers in Figure 14). On the other hand, weighting the measured temperature in terms of the mass flow rate, accounts only for the thermal energy escaping the cylinder during the EVO event, thus providing a more accurate measure of the average temperature during the cycle.

The effect of using a mass-average temperature on the calculated exhaust enthalpy flow can be seen in Figure 15 for the two speed/load conditions presented above. The time-average enthalpy flow is calculated using Equation 9, and the mass-average enthalpy flow using Equation 12. These results show that the exhaust enthalpy flow is increased by 15 % and 18 %, for the low and high load cases respectively, when calculated on a mass-average basis. When this increase is considered into the first law analysis, an increase of ~5 percentage points in normalised exhaust energy is observed, as can be seen in Figure 16 and Figure 17. This consequently reduces the extraneous losses by the same amount which reduces the uncertainty associated with the first law analysis model.

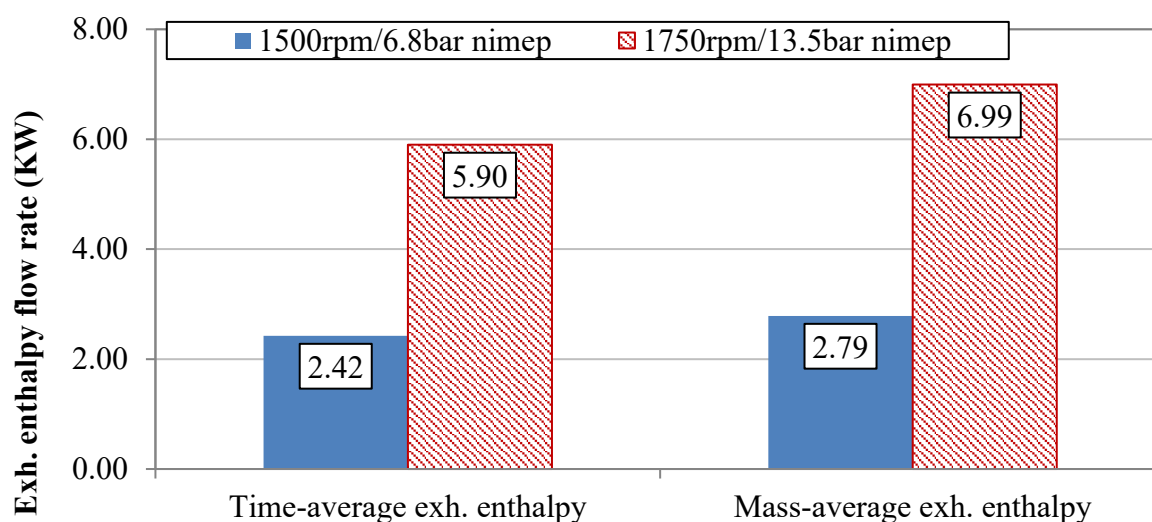


Figure 15: Comparison of time (Equation 9) and mass-average (Equation 12) exhaust enthalpy flow rate under two speed/load conditions.

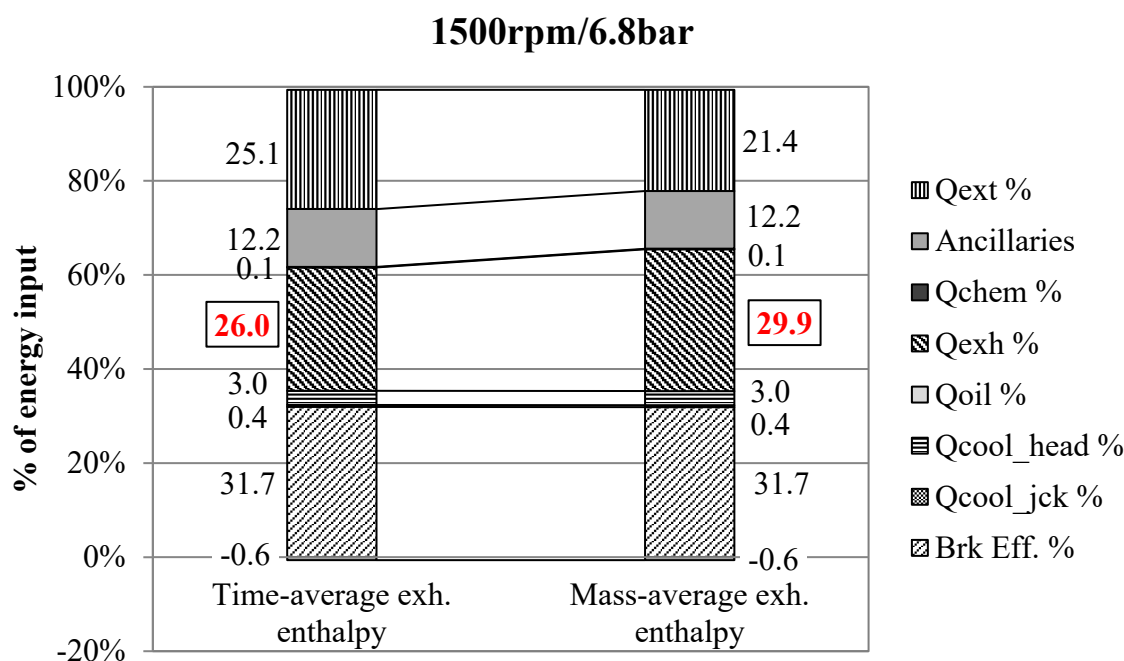


Figure 16: Effect of mass-average exhaust enthalpy on energy balance results for the 1500rpm/6.8bar nIMEP case.

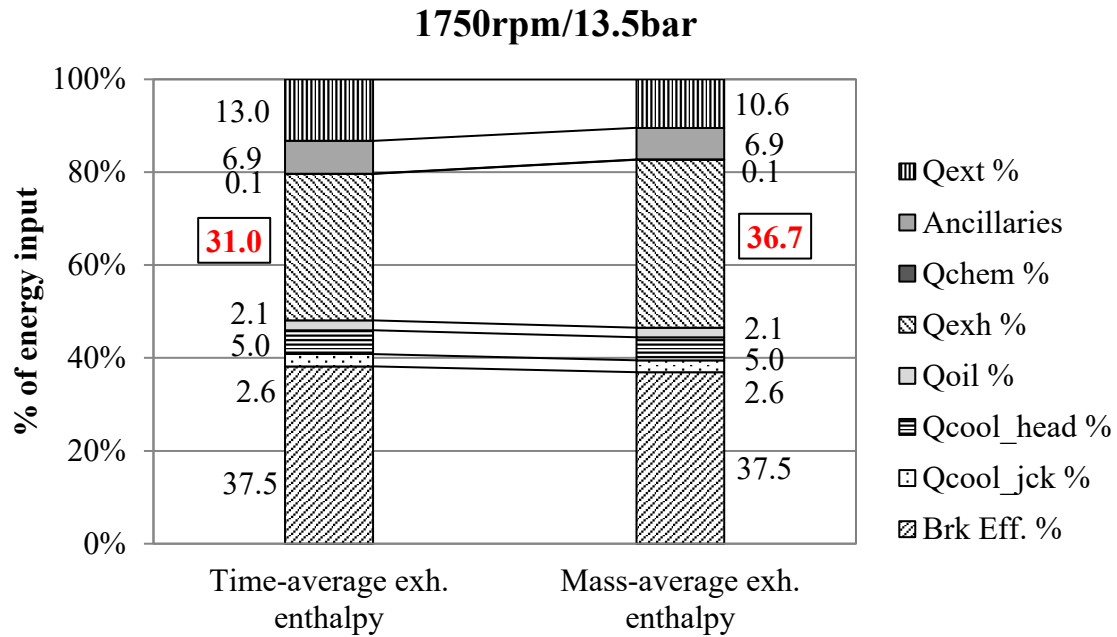


Figure 17: Effect of mass-average exhaust enthalpy on energy balance results for the 1750rpm/13.5bar nIMEP case.

These findings are important since they indicate that common measurement practices can lead to misleading observations. An indication of the “true” exhaust temperature, using the reconstruction method presented above, despite providing an accurate indication of the instantaneous temperature during the cycle can still result in an under prediction of exhaust enthalpy flow, if calculated on time-average terms. A mass-average calculation alleviates these issues. However, it is acknowledged that knowledge of the instantaneous mass-flow rate is usually only available through numerical simulation and as such, on-engine applications might require the use of time-average terms. This work informs on the expected magnitude of error in such applications.

Conclusions

This work presented a temperature reconstruction method to recover the “true” temperature signal from thermocouple sensors, by correcting the inherent dynamic, conduction and radiation errors associated with the measurement process. The reconstruction method uses the signals of two different size thermocouples and was validated using simulated signals produced using a lumped capacitance model. Overall, the temperature reconstruction method put forward predicts the “true” gas temperature very well, for both speed/load conditions tested. To summarise this work has shown that:

1. The maximum temperature error is reduced by as much as 14 percentage points when the proposed reconstruction method is used.
2. The smaller size thermocouples will produce a more accurate reconstruction signal
3. Estimating average exhaust temperature on a mass-average basis provides better indication of exhaust temperature.
4. Calculating the exhaust enthalpy on a mass-average basis improves the accuracy of the energy balance method and results in an increase in normalized exhaust energy of 5 percentage points

The results of the proposed reconstruction method indicate that this technique offers a clear benefit when trying to estimate the exhaust enthalpy more accurately. Since this method was only validated with simulated thermocouple signals the next step would be to be used on experimental data. However, care should be taken, as this technique is very sensitive to signal noise and the averaging process which can affect the reconstruction quality. Therefore, the best compromise between a clean signal and loss of signal information needs to be found with appropriate filtering.

References

- [1] Papaioannou, N., Leach, F. C., Davy, M. H., Weall, A., & Cooper, B. (2019). Evaluation of exhaust gas recirculation techniques on a high-speed direct injection diesel engine using first law analysis. *Proceedings of the Institution of*

- [2] Dahlstrom, J., Andersson, O., Tuner, M., and Persson, H., "Experimental Comparison of Heat Losses in Stepped-Bowl and Re-Entrant Combustion Chambers in a Light Duty Diesel Engine," SAE Technical Paper 2016-01-0732, 2016, <https://doi.org/10.4271/2016-01-0732>.
- [3] Olmeda, P., Martin, J., Garcia, A., Blanco, D. et al., "Evaluation of EGR Effect on the Global Energy Balance of a High Speed DI Diesel Engine," SAE Technical Paper 2016-01-0646, 2016, <https://doi.org/10.4271/2016-01-0646>.
- [4] Smith, L., Preston, W., Dowd, G., Taylor, O. et al., "Application of a First Law Heat Balance Method to a Turbocharged Automotive Diesel Engine," SAE Technical Paper 2009-01-2744, 2009, <https://doi.org/10.4271/2009-01-2744>.
- [5] Caton, J., "Comparisons of Thermocouple, Time-Averaged and Mass-Averaged Exhaust Gas Temperatures for a Spark-Ignited Engine," SAE Technical Paper 820050, 1982, <https://doi.org/10.4271/820050>.
- [6] Papaioannou, N., Leach, F., and Davy, M., "Thermal Analysis of Steel and Aluminium Pistons for an HSDI Diesel Engine," SAE Technical Paper 2019-01-0546, 2019, <https://doi.org/10.4271/2019-01-0546>.
- [7] G.C. Mavropoulos (December 22nd 2011). Unsteady Heat Conduction Phenomena in Internal Combustion Engine Chamber and Exhaust Manifold Surfaces, Heat Transfer - Engineering Applications, Vyacheslav S. Vikhrenko, IntechOpen, DOI: 10.5772/26369.
- [8] Zhao, H., Laser diagnostics and optical measurement techniques in internal combustion engines. 2012: SAE International.
- [9] Förster, F.J., et al., Time-resolved gas thermometry by laser-induced grating spectroscopy with a high-repetition rate laser system. Experiments in Fluids, 2017. 58(7): p. 87. <https://doi.org/10.1007/s00348-017-2370-6>
- [10] Scott, B., Willman, C., Williams, B., Ewart, P. et al., "In-Cylinder Temperature Measurements Using Laser Induced Grating Spectroscopy and Two-Colour PLIF," SAE Int. J. Engines 10(4):2191-2201, 2017, <https://doi.org/10.4271/2017-24-0045>.
- [11] West, W.E. and J.W. Westwater, Radiation-Conduction Correction for Temperature Measurements in Hot Gases. Industrial & Engineering Chemistry, 1953. 45(10): p. 2152-2156. DOI: 10.1021/ie50526a022
- [12] Bradley, D. and K.J. Matthews, Measurement of High Gas Temperatures with Fine Wire Thermocouples. Journal of Mechanical Engineering Science, 1968. 10(4): p. 299-305. <https://doi.org/10.1243%2FJMES.JOUR.1968.010.048.02>
- [13] Shaddix, C.R. *Correcting thermocouple measurements for radiation loss: A critical review*. United States: N. p., 1999. Web.
- [14] Kobus, C.J., *True fluid temperature reconstruction compensating for conduction error in the temperature measurement of steady fluid flows*. Review of Scientific Instruments, 2006. 77(3): p. 034903. <https://doi.org/10.1063/1.2186211>
- [15] Papaioannou, N., Leach, F., and Davy, M., "Effect of Thermocouple Size on the Measurement of Exhaust Gas Temperature in Internal Combustion Engines," SAE Technical Paper 2018-01-1765, 2018, <https://doi.org/10.4271/2018-01-1765>.
- [16] Khine, S.M., T. Houra, and M. Tagawa, *Heat-conduction error of temperature sensors in a fluid flow with nonuniform and unsteady temperature distribution*. Review of Scientific Instruments, 2013. 84(4): p. 044902. <https://doi.org/10.1063/1.4801853>
- [17] Kar, K., Roberts, S., Stone, R., Oldfield, M. et al., "Instantaneous Exhaust Temperature Measurements Using Thermocouple Compensation Techniques," SAE Technical Paper 2004-01-1418, 2004, <https://doi.org/10.4271/2004-01-1418>.
- [18] Tagawa, M. and Y. Ohta, *Two-thermocouple probe for fluctuating temperature measurement in combustion—Rational estimation of mean and fluctuating time constants*. Combustion and Flame, 1997. 109(4): p. 549-560. [https://doi.org/10.1016/S0010-2180\(97\)00044-8](https://doi.org/10.1016/S0010-2180(97)00044-8)
- [19] Forney, L.J. and G.C. Fralick, *Three-wire thermocouple: Frequency response in constant flow*. Review of Scientific Instruments, 1995. 66(5): p. 3331-3336. <https://doi.org/10.1063/1.1145503>
- [20] Kee, Robert J., et al. "Fast Response Exhaust Gas Temperature Measurement in IC Engines." SAE Transactions, vol. 115, 2006, pp. 598–609. JSTOR, www.jstor.org/stable/44700089.
- [21] Kar, K., Swain, A. K., and Raine, R. (December 5, 2008). "Identification of Time-Varying Time Constants of Thermocouple Sensors and Its Application to Temperature Measurement." ASME. J. Dyn. Sys., Meas., Control. January 2009; 131(1): 011005. <https://doi.org/10.1115/1.3023111>
- [22] Whitaker, S., *Forced convection heat transfer correlations for flow in pipes, past flat plates, single cylinders, single spheres, and for flow in packed beds and tube bundles*. AIChE Journal, 1972. 18(2): p. 361-371. <https://doi.org/10.1002/aic.690180219>
- [23] Gamma Technologies, <https://www.gtisoft.com/>. [cited 2019].
- [24] Ross, S.M., *Introduction to probability and statistics for engineers and scientists*. 1987, New York: John Wiley and Sons.

Contact Information

Felix Leach

Department of Engineering Science, University of Oxford, Parks Rd, Oxford, OX1 3PJ, UK

Email: felix.leach@eng.ox.ac.uk

Acknowledgments

The authors would like to thank the Jaguar Land Rover Limited and University of Oxford John Fell fund for financial support. Nick Papaioannou would like to thank EPSRC for supporting his research (Grant number: 1515450).

Definitions/Abbreviations

A_{csa}	Cross-sectional area of thermocouple wire
A_s	Surface area of thermocouple junction
CAD	Crank Angle Degrees
c_p	Heat capacity of thermocouple junction
EGT	Exhaust Gas Temperature
EVC	Exhaust Valve Closing
EVO	Exhaust Valve Opening
h	Convective heat transfer coefficient
ICE	Internal Combustion Engine
k	Thermal conductivity
L	Conduction length
m	Mass of thermocouple junction
\bar{m}_{exh}	Time-average mass flow rate of exhaust gases
$\dot{m}_{exh}(\theta)$	Instantaneous mass flow rate of exhaust gases
NIMEP	Net Indicated Mean Effective Pressure
PMEP	Pumping Mean Effective Pressure
\bar{Q}_{exh}	Time-average energy transfer rate to exhaust
\hat{Q}_{exh}	Mass-average energy transfer rate to exhaust
T_c	Temperature of reference junction
\bar{T}_{exh}	Time-average temperature of exhaust gases
\hat{T}_{exh}	Mass-average temperature of exhaust gases
T_g	Instantaneous exhaust gas temperature
T_{ref}	Temperature of 3 mm sheathed thermocouple
T_s	Thermocouple junction temperature
T_w	Exhaust pipe wall temperature
T_0	Inlet temperature
T2	Temperature of 50.8 μm thermocouple
T5	Temperature of 127 μm thermocouple
T10	Temperature of 254 μm thermocouple
ε	Emissivity of thermocouple junction
ζ	Weight factor for exponential moving averaging
σ	Stefan-Boltzmann constant
τ	Time-constant